

A unified analysis of convex and non-convex ℓ_p -ball projection problems

Joong-Ho Won¹, Kenneth Lange², and Jason Xu³

¹Seoul National University

²University of California, Los Angeles

³Duke University

Abstract

The task of projecting onto ℓ_p norm balls is ubiquitous in statistics and machine learning, yet the availability of actionable algorithms for doing so is largely limited to the special cases of $p = \{0, 1, 2, \infty\}$. In this paper, we introduce novel, scalable methods for projecting onto the ℓ_p ball for general $p > 0$. For $p \geq 1$, we solve the univariate Lagrangian dual via a dual Newton method. We then carefully design a bisection approach for $p < 1$, presenting theoretical and empirical evidence of zero or a small duality gap in the non-convex case. The success of our contributions is thoroughly assessed empirically, and applied to large-scale regularized multi-task learning and compressed sensing.

1 Introduction

The goal of this paper is to develop and analyze efficient algorithms for projecting a point \mathbf{y} in Euclidean space \mathbb{R}^d onto an ℓ_p “norm ball” of radius r . Projection seeks the closest point in the ball, solving the problem

$$\min_{\mathbf{x} \in \mathbb{R}^d} \frac{1}{2} \|\mathbf{x} - \mathbf{y}\|_2^2 \quad \text{subject to} \quad \|\mathbf{x}\|_p \leq r, \quad (\text{P})$$

where $\|\mathbf{v}\|_p = (\sum_{i=1}^d |v_i|^p)^{1/p}$ denotes the ℓ_p “norm” of a vector $\mathbf{v} \in \mathbb{R}^d$. If the power $p \geq 1$, then $\|\mathbf{v}\|_p$ is a proper norm, and (P) is a convex optimization problem. Otherwise, $\|\mathbf{v}\|_p$ defines only a quasi-norm, and the problem becomes non-convex. Throughout, we maintain the term “norm” even if $p \in [0, 1)$, for nomenclatural convenience. Writing the norm-ball constraint set as rB_p , the solution to (P) is the projection denoted $P_{rB_p}(\mathbf{y})$.

Projecting onto ℓ_p norm balls plays a key role in some of the most prominent inverse problems in machine learning, signal processing, and statistics. The canonical setting of minimizing a measure of a fit subject to a constraint on solution complexity measured

by a norm (Candes and Tao, 2005; Donoho, 2006) arises, for instance, in compressed sensing. If $\phi(\mathbf{x}; \mathbf{y})$ measures the goodness of fit of model parameter \mathbf{x} to given data \mathbf{y} , then the problem is stated

$$\min_{\mathbf{x} \in \mathbb{R}^d} \phi(\mathbf{x}; \mathbf{y}) \quad \text{subject to} \quad \|\mathbf{x}\| \leq r. \quad (1)$$

Among the popular choices of the norm $\|\cdot\|$ are the ℓ_p norms and $\ell_{1,p}$ mixed norms denoted $\|\mathbf{x}\|_{1,p} = \sum_{g=1}^G \|\mathbf{x}_g\|_p$, where \mathbf{x} is partitioned into subvectors indexed by g . The ℓ_2 norm is used in Tikhonov regularization or ridge regression. Bridge regression (Fu, 1998) uses an ℓ_p norm optimized over $p \in (1, 2)$. The ℓ_1 norm is the most widely used regularizer in sparse learning (Tibshirani et al., 2015). In compressed sensing, exact signal recovery can be accomplished with fewer measurements under non-convex ℓ_p norms ($0 < p < 1$) compared to the ℓ_1 norm (Wang et al., 2011).

Whatever the choice of p , algorithms for solving problem (1) routinely require solving projection (P) as a subproblem. For instance, if ϕ is smooth, projected gradient descent iterates via the sequence $\mathbf{x}_{k+1} = P_{rB_p}[\mathbf{x}_k - \eta_k \nabla \phi(\mathbf{x}_k)]$. In multi-task learning (Argyriou et al., 2008; Sra, 2012; Vogt and Roth, 2012), the use of the $\ell_{1,2}$ (“group lasso”) (Yuan and Lin, 2006; Meier et al., 2008) or $\ell_{1,\infty}$ norms (Liu et al., 2009; Quattoni et al., 2009) is popular, while an $\ell_{1,p}$ norm with $p \in (1, \infty]$ chosen in a data-adaptive fashion has been shown to significantly improve performance (Zhang et al., 2010). Projection onto an $\ell_{1,p}$ norm ball for solving problem (1) separates into G instances of (P). Hence efficiently solving (P) for various values of $p > 0$ is instrumental to solving problems of type (1).

However, algorithms for solving (P) are quite limited to a few special values of p . Projecting onto the ℓ_2 or ℓ_∞ ball is trivial, and fast algorithms are available for the ℓ_1 ball (Duchi et al., 2008; Condat, 2016). For general convex settings ($p > 1$), problem (P) has been studied mostly as a subproblem of $\ell_{1,p}$ mixed norm regularization (Liu and Ye, 2010; Zhou et al., 2015; Barbero and Sra, 2018). A common approach is to formulate (P) as an unconstrained problem

$$\min_{\mathbf{x} \in \mathbb{R}^d} f_0(\mathbf{x}) + \iota_{rB_p}(\mathbf{x}), \quad (P')$$

where $f_0(\mathbf{x}) = \frac{1}{2} \|\mathbf{x} - \mathbf{y}\|_2^2$, and ι_C is the $0/\infty$ indicator function of set C . Problem (P') can be solved via its Fenchel (or Lagrange) dual

$$\min_{\mathbf{z}} \frac{1}{2} \|\mathbf{z} - \mathbf{y}\|_2^2 + r \|\mathbf{z}\|_q, \quad \text{where} \quad \frac{1}{p} + \frac{1}{q} = 1, \quad (F)$$

whose solution is the proximal operator of the dual norm $\mathbf{z}^* = \text{prox}_{r\|\cdot\|_q}(\mathbf{y})$. The solution $P_{rB_p}(\mathbf{y})$ to (P) is then recovered by Moreau’s decomposition $\mathbf{y} = P_{rB_p}(\mathbf{y}) + \mathbf{z}^*$. The technical report Liu and Ye (2010) explored some properties of problem (F), and proposed a double-bisection method implemented in the popular software package SLEP (Liu et al., 2011). Recently, Barbero and Sra Barbero and Sra (2018) proposed solving (F) via the projected Newton method (Bertsekas, 1982). The major difficulty with (F) is its nonsmoothness. As we will detail in Section 5, the analysis of Liu and Ye (2010) entails opaque auxiliary functions, not to mention slowness and poor

scalability of the double-bisection method. As discussed in the sequel, the method of Barbero and Sra Barbero and Sra (2018) suffers from numerical instability when p is large. In the non-convex regime, available projection methods are limited. Bahmani and Raj (2013) studies basic theoretical properties of projected points. In Das Gupta and Kumar (2013), an exhaustive search is attempted. More recent efforts include Chen et al. (2021) and Yang et al. (2021).

In this paper, we provide a unified treatment of both convex and non-convex instances of the projection problem (P). Our approach is to reformulate (P) using the p th power as

$$\min_{\mathbf{x} \in \mathbb{R}^d} f_0(\mathbf{x}) \quad \text{subject to} \quad \frac{1}{p}(\|\mathbf{x}\|_p^p - r^p) \leq 0. \quad (\text{P}'')$$

Then, the Lagrange dual of (P'') is

$$\max_{\mu \geq 0} g(\mu) \triangleq \inf_{\mathbf{x} \in \mathbb{R}^d} \mathcal{L}(\mathbf{x}, \mu), \quad \text{where} \quad \mathcal{L}(\mathbf{x}, \mu) = f_0(\mathbf{x}) + \frac{\mu}{p} \left(\sum_{i=1}^d |x_i|^p - r^p \right). \quad (\text{D})$$

If $\mathbf{x}^*(\mu)$ minimizes $\mathcal{L}(\mathbf{x}, \mu)$ and μ^* maximizes $g(\mu)$, then $P_{rB_p}(\mathbf{y}) = \mathbf{x}^*(\mu^*)$. Compared to the Fenchel dual (F), the present formulation (D) has three key advantages: 1) the Lagrangian \mathcal{L} is separable in \mathbf{x} ; 2) the dual objective function g is twice continuously differentiable if $p > 1$, and hence is amenable to Newton methods for maximization; 3) it is *univariate* and well-defined even when $0 < p < 1$. In the latter setting, minimization of the Lagrangian $\mathcal{L}(\mathbf{x}, \mu)$ with respect to \mathbf{x} , namely evaluation of $g(\mu)$, is relatively well-studied under the name of non-convex ℓ_p regularization (Marjanovic and Solo, 2012; Xu et al., 2012; Chartrand and Yin, 2016; Yukawa and Amari, 2016; Hu et al., 2017), compared to problem (P). Since $g(\mu)$ is concave regardless of p , in principle any univariate maximization strategy for g can be used to solve (D).

Though strong duality is not guaranteed when $0 < p < 1$, we show that a carefully designed bisection method yields accurate solutions to (P) with very small duality gaps. For convex cases, we show that our Newton method achieves a quadratic rate of convergence, with no projection onto the set $\{\mu : \mu \geq 0\}$ needed. Fast convergence is paramount because (P) is commonly used as a building block within iterative algorithms for more complex tasks, such as problem (1). The success of our methods hinges on fast and accurate evaluation of the associated univariate proximal map, which we closely analyze in the following sections. Our primary contribution is recognizing the value of formulation (D) together with carefully executed analyses of the proximal map for both convex and non-convex cases.

The paper is organized as follows. After analyzing the properties of (P), (D), and the associated proximal maps in Section 2, we propose a dual Newton method for $p > 1$ and establish its convergence rate in Section 3. Next, Section 4 details the viable alternative of bisection for non-convex cases. Related methods are discussed in Section 5. In Section 6, the algorithms are thoroughly assessed via simulation. Together they comprise a suite that allows for successful projection onto general ℓ_p balls. The empirical study also illustrates the key role of such projections within algorithms such as projected and proximal gradient (Beck and Teboulle, 2009), applied to multi-task learning and compressed sensing.

2 Evaluating dual objective via associated proximal map

2.1 Basic properties of the ℓ_p -ball projection

In this section, we study how to represent and evaluate the dual objective $g(\mu)$ of problem (D) in terms of the associated univariate proximal maps. We begin with a few simple observations when \mathbf{y} is external to the ball rB_p , given in (Bahmani and Raj, 2013):¹

1. The projected point \mathbf{x} is a boundary point in the sense that $\|\mathbf{x}\|_p = r$.
2. The components of \mathbf{x} have the same signs as the corresponding components of \mathbf{y} .
3. No component x_i of \mathbf{x} can satisfy $|x_i| > |y_i|$, and if $y_i = 0$, then $x_i = 0$.
4. No two components x_i and x_j of \mathbf{x} can satisfy $|x_i| > |x_j|$ when $|y_i| < |y_j|$.
5. We can take the radius r of the ball to be 1. Indeed, if $r^{-1}\mathbf{x}$ solves the corresponding problem for the unit ball and the external point $r^{-1}\mathbf{y}$, then \mathbf{x} solves the original problem.

Henceforth, we take $\mathbf{y} > \mathbf{0}$ (denoting elementwise inequality), $r = 1$, and $\|\mathbf{y}\|_p > 1$ without loss of generality.

2.2 Univariate proximal map for problem (D)

As stated, evaluating the dual objective $g(\mu)$ in problem (D) requires minimizing the Lagrangian $\mathcal{L}(\mathbf{x}, \mu)$ over \mathbf{x} (with $r = 1$). The latter problem is equivalent to the ℓ_p -regularized least squares problem

$$\min_{\mathbf{x}} \frac{1}{2} \|\mathbf{x} - \mathbf{y}\|_2^2 + \frac{\mu}{p} \|\mathbf{x}\|_p^p,$$

in which the p th power of the ℓ_p norm satisfies the triangle inequality when $0 < p < 1$ (Chartrand and Yin, 2016). For any p , this problem is separable in the coordinates of $\mathbf{x} = (x_1, \dots, x_d)$, and it suffices to minimize the univariate function

$$f_\mu(x; y) \triangleq \frac{1}{2}(x - y)^2 + \frac{\mu}{p}|x|^p \tag{2}$$

for each $y = y_i$. If we define $s_p(x) \triangleq \frac{1}{p}|x|^p$, then the minimizer of $f_\mu(x; y)$ is just the proximal map $\text{prox}_{\mu s_p}(y)$ of μs_p , that is,

$$\text{prox}_{\mu s_p}(y) \triangleq \underset{x}{\operatorname{argmin}} \left\{ \frac{1}{2}(x - y)^2 + \frac{\mu}{p}|x|^p \right\}$$

for $\mu \geq 0$. If $p \geq 1$, then $\text{prox}_{\mu s_p}(y)$ is unique. However, when $p < 1$, it may be set-valued; see Section 2.4.2 for details.

¹These properties have emerged in the context of studying theoretical properties of projected gradient descent for ℓ_p -norm constrained least squares (problem (1) with $\phi(\mathbf{x}, \mathbf{y}) = \frac{1}{2}\|\mathbf{y} - \mathbf{A}\mathbf{x}\|_2^2$). However, no actual algorithm for ℓ_p -ball projection is provided in Bahmani and Raj (2013).

2.3 The univariate dual

From the discussion in the preceding section, the dual objective $g(\mu)$ in (D) can be written

$$g(\mu) = \frac{1}{2} \sum_{i=1}^d [y_i - x_i^*(\mu)]^2 + \frac{\mu}{p} \sum_{i=1}^d |x_i^*(\mu)|^p - \frac{\mu}{p} \quad (3)$$

where $x_i^*(\mu) = \text{prox}_{\mu s_p}(y_i)$. Even though the latter proximal map is set-valued when $0 < p < 1$, $g(\mu)$ is always single-valued, since any element of the set $\mathbf{x}^*(\mu) = x_1^*(\mu) \times \dots \times x_d^*(\mu)$ globally minimizes $\mathcal{L}(\mathbf{x}, \mu)$.

We now examine the domain of g . A nonzero minimizer of $f_\mu(x_i; y_i)$ in formula (2), i.e., if $x_i = \text{prox}_{\mu s_p}(y_i) > 0$, satisfies the stationary condition

$$0 = x_i - y_i + \mu x_i^{p-1}. \quad (4)$$

(Recall that $y_i > 0$ is assumed without loss of generality.) Now, multiply equation (4) by x_i and sum over all i (so that the zero minimizer $x_i = 0$ is allowed even if equation (4) is satisfied). These actions produce

$$0 = \|\mathbf{x}\|_2^2 - \mathbf{y}^T \mathbf{x} + \mu \|\mathbf{x}\|_p^p, \quad (5)$$

which in turn yields $\mu = \mathbf{y}^T \mathbf{x} - \|\mathbf{x}\|_2^2$ for $\|\mathbf{x}\|_p = 1$ (recall that we assume $r = 1$ and $\|\mathbf{y}\|_p > 1$; the optimum occurs at the boundary of the constraint set). Note a generalization of equation (5) is studied in Chen et al. (2013); Lu (2014) for ℓ_p -regularization problems and their extensions. Note that μ so defined is automatically nonnegative; μ is positive so long as $0 < |x_i| < |y_i|$ for some i . The formula for μ also yields an upper bound through Hölder's inequality: if $p \geq 1$, $\mu \leq \mathbf{y}^T \mathbf{x} \leq \|\mathbf{y}\|_q \|\mathbf{x}\|_p = \|\mathbf{y}\|_q$, where $1/p + 1/q = 1$. If $p \in (0, 1)$, then $\mu \leq \mathbf{y}^T \mathbf{x} \leq \|\mathbf{y}\|_\infty \|\mathbf{x}\|_1 \leq \|\mathbf{y}\|_\infty$, since $\|\mathbf{x}\|_p \leq 1$ implies $\|\mathbf{x}\|_1 \leq 1$. Thus, it suffices to maximize $g(\mu)$ on $[0, \|\mathbf{y}\|_q]$, where $\frac{1}{p} + \frac{1}{q} = 1$ or $q = \infty$.

2.4 Analysis and computation of the proximal map

2.4.1 Convex case ($p > 1$)

Newton's method The objective $f_\mu(x; y) = \frac{1}{2}(y - x)^2 + \mu s_p(x)$ of (2) is twice continuously differentiable on $[0, y]$ for $p > 1$. Thus, $\text{prox}_{\mu s_p}(y)$ can be evaluated via Newton's method. The updates amount to

$$x_{n+1} = \frac{y + \mu(p-2)|x_n|^{p-1} \text{sgn}(x_n)}{1 + \mu(p-1)|x_n|^{p-2}} = \frac{y/|x_n|^{p-2} + \mu(p-2)x_n}{1/|x_n|^{p-2} + \mu(p-1)}. \quad (6)$$

Whenever $p \geq 2$ and $y \geq 0$, *all iterates remain in* $[0, y]$, and convergence is guaranteed as the derivative $f'_\mu(x; y) = x - y + \mu x^{p-1}$ is convex in $x \geq 0$. Numerical overflows are still a consideration for very large values of p . Both forms in (6) are pertinent in this regard: the latter is numerically stable when $|x_n| > 1$ while the former is preferable when $|x_n| < 1$. If the quantity $\mu|y|^{p-1}$ falls below machine precision, it is safe to set $\text{prox}_{\mu s_p}(y) = y$. When $1 < p < 2$, the iterates x_n defined above may fall below 0.

To avoid this, we may appeal to Moreau's decomposition that tells us that we may equivalently compute

$$y - \mu \operatorname{prox}_{\mu^{-1}s_p^*}(\mu^{-1}y),$$

where

$$s_p^*(z) = \sup_x \{xz - s_p(x)\} = \frac{1}{q}|y|^q = s_q(y), \quad q = \frac{p}{p-1}$$

is the Fenchel conjugate of s_p . Since $q > 2$, applying Newton's method on s_q avoids the issue. Again numerical caution is required when $\mu^{-1}|\mu^{-1}y|^{q-1} = \mu^{-1}|\mu^{-1}y|^{1/(p-1)}$ nearly vanishes, for in this case $x^*(\mu) = \operatorname{prox}_{\mu s_p}(y) = y - \mu \operatorname{prox}_{\mu^{-1}s_q}(\mu^{-1}y) \approx y - y = 0$, but $f'_\mu(0; y) = -y \neq 0$. Even though $x^*(\mu)$ is very close to zero beyond numerical precision, $|x^*(\mu)|^{p-1}$ may be close to 1 when $p \rightarrow 1$. It is therefore safe to set

$$|x^*(\mu)|^{p-1} = |\mu^{-1}y| \tag{7}$$

and $x^*(\mu) = \operatorname{sgn}(y)|\mu^{-1}y|^{1/(p-1)}$.

Initial point Toward computing the proximal map, we suggest initializing x by $x_0 = \max\{1, \min(y, [y + \mu(p-2)]/[1 + \mu(p-1)])\}$ based on the following observation. When $p > 1$ is very large, the behavior of the term $\mu|x|^{p-1}$ radically changes from near 0 to near ∞ as we pass from $|x| < 1$ to $|x| > 1$, the value $\operatorname{prox}_{\mu s_p}(y)$ tends to be close to 1. Based on the sign of $f'_\mu(1; y) = 1 - y + \mu$, the proximal value is less than 1 if $0 \leq y < 1 + \mu$. The convexity of $f'_\mu(x; y)$ allows initializing the Newton algorithm with $x = 1$. Now consider letting $x_0 = 1 + \epsilon$ for ϵ small. We then have that

$$y - 1 - \epsilon = \mu(1 + \epsilon)^{p-1} \approx \mu[1 + (p-1)\epsilon].$$

Rearranging this approximate equality yields

$$1 + \epsilon \approx \frac{y + \mu(p-2)}{1 + \mu(p-1)}.$$

This quantity is greater than 1 if $y > 1 + \mu$ and less than y whenever $y > (p-2)/(p-1)$.

2.4.2 Non-convex case

As claimed, the proximal map $\operatorname{prox}_{\mu s_p}$ can be set-valued if $p < 1$:

Proposition 1 (Marjanovic and Solo (2012), Theorem 1²) *Let $z_p(y)$ be the implicit function defined as the root of equation $0 = x - y + x^{p-1}$ greater than $m_p = (1-p)^{1/(2-p)}$, where $p \in (0, 1)$ and $y \geq 0$. Then the proximal map of μs_p , where $\mu \geq 0$, is given by*

$$\operatorname{prox}_{\mu s_p}(y) = \begin{cases} 0, & \text{if } 0 \leq y < \mu^{1/(2-p)}r_p, \\ \{0, y\kappa_p/r_p\}, & \text{if } y = \mu^{1/(2-p)}r_p, \\ \mu^{1/(2-p)}z_p(\mu^{-1/(2-p)}y), & \text{if } y > \mu^{1/(2-p)}r_p, \end{cases} \tag{8}$$

where $\kappa_p = (2/p)^{1/(2-p)}m_p = [2(1-p)/p]^{1/(2-p)}$, and $r_p = \kappa_p + \kappa_p^{p-1}$. Furthermore, $z(r_p) = \kappa_p$.

Remark 1 *The following can be easily shown:*

1. $\lim_{p \downarrow 0} r_p = \infty$ and $\lim_{p \rightarrow 1} r_p = 1$;
2. $\lim_{p \downarrow 0} \frac{r_p}{\sqrt{2/p}} = 1$ and $\lim_{p \downarrow 0} \frac{\kappa_p}{\sqrt{2/p}} = 1$;
3. $\lim_{p \downarrow 0} \max_{y \geq r_p} [y - z_p(y)] = 0$, and $\lim_{p \rightarrow 1} \max_{y \geq r_p} [y - z_p(y)] = 1$;
4. $\lim_{y \rightarrow \infty} \frac{y - z_p(y)}{1/y^{1-p}} = 1$.

Thus if $p \downarrow 0$, then $\text{prox}_{\mu s_p}(y)$ tends to the hard thresholding operator

$$\underset{x \in \mathbb{R}}{\text{argmin}} \left\{ \frac{1}{2}(x - y)^2 + \frac{\mu}{p}|x|_0 \right\} = \begin{cases} 0, & |y| < \sqrt{2\mu/p}, \\ \{0, \sqrt{2\mu/p}\}, & |y| = \sqrt{2\mu/p}, \\ y, & |y| > \sqrt{2\mu/p}, \end{cases} \quad (9)$$

where $|x|_0 = 0$ if $x = 0$ and 1 otherwise. When p tends to 1, it converges to the soft thresholding operator

$$\underset{x \in \mathbb{R}}{\text{argmin}} \left\{ \frac{1}{2}(x - y)^2 + \mu|x| \right\} = \begin{cases} 0, & |y| \leq \mu, \\ \text{sgn}(y)(|y| - \mu), & |y| > \mu. \end{cases}$$

Proposition 1 suggests that computing $z_p(y)$, or the root of the equation $0 = x - y + x^{p-1}$ that is greater than $m_p = (1-p)^{1/(2-p)}$, with high accuracy is a key to computing the set-valued map $\text{prox}_{\mu s_p}(y)$ (for $y \geq 0$), when $p \in (0, 1)$. This root is a potential minimizer of $f_1(x; y) = \frac{1}{2}(x - y)^2 + |x|^p/p$, which we abbreviate as $f(x)$ for simplicity, on $x \geq 0$. Its derivative $f'(x) = x - y + x^{p-1}$ is infinite at $x = 0$ and convex on $x > 0$. The minimum of $f'(x)$ occurs at $m_p = (1-p)^{1/(2-p)}$ that is strictly positive. If $f'(m_p)$ is non-negative (which means $y \leq m_p + m_p^{p-1}$), then the minimum of $f(x)$ occurs at $x = 0$. Otherwise, $y \geq m_p + m_p^{p-1}$, and the minimum occurs to the right of m_p . Since $f'(x)$ is strictly increasing on (m_p, ∞) and $f'(y) = y^{p-1}$, it must have a unique zero $z_p(y)$ in the interval (m_p, y) . It follows that $z_p(y)$ and 0 contend for the minimum point of $f(x)$. Determining which only requires comparing two quantities $f(z_p(y))$ and $f(0) = \frac{1}{2}y^2$. Hence the r_p in Proposition 1 needs not be computed.

Newton's method In computing $z_p(y)$, the Newton method (6) can be employed without any modification. This iteration necessarily converges to $z_p(y)$ from *any* initial point in (m_p, y) since $f'(x)$ is increasing and convex in this interval. Since the convexity of $f'(x) = f'_1(x; y)$ remains intact with $p \in (0, 1)$, the choice of the initial point in the $p \geq 2$ case is still valid. From Remark 1, we see that if $\kappa_p/\sqrt{2/p}$ is very close to 1 beyond the machine precision, it is safe to approximate the proximal map with hard thresholding (9).

Remark 2 *For $p = 1/2$ and $p = 2/3$, it can be shown that $z_p(y)$ has a closed form, so does $\text{prox}_{\mu s_p}(y)$ (Xu et al., 2012; Chartrand and Yin, 2016). Our goal here is, however, to provide a unifying strategy of evaluating the dual function $g(\mu)$, for a wide range of p .*

Algorithm The discussion in this section is summarized in Algorithm 1.

Algorithm 1 Compute $\text{prox}_{\mu s_p}(y)$ for $s_p(x) = |x|^p/p$, $p \in (0, \infty) \setminus \{1, 2, \infty\}$

Input: $y > 0$, $\mu \geq 0$, and $p > 0$

if $p > 2$ **then**

$x^* \leftarrow \text{NewtonRoot}(y, \mu, p)$

end if

if $p > 1$ **then**

if $\mu^{-1}(y/\mu)^{\frac{1}{1-p}} \approx 0$ **then**

return $(y/\mu)^{\frac{1}{p-1}}$

end if

$q \leftarrow 1/(1 - 1/p)$

$z \leftarrow \text{NetwonProx}(y/\mu, 1/\mu, q)$

return $y - \mu z$

else

$x_{\min} \leftarrow [(1 - p)\mu]^{1/(2-p)}$

if $f'_\mu(x_{\min}; y) < 0$ **then**

$z \leftarrow \text{NewtonRoot}(y, \mu, p)$

return $\text{argmin}_{x \in \{0, z\}} f(x; y)$

else

return 0

end if

end if

Subroutine NewtonRoot:

if $\mu y^{p-1} \approx 0$ **then**

return y

end if

$x \leftarrow \max\{1, \min(y, [y + \mu(p-2)]/[1 + \mu(p-1)])\}$

repeat

if $x > 1$ or $p < 1$ **then**

$a \leftarrow y/x^{p-2} + \mu(p-2)x$

$b \leftarrow 1/x^{p-2} + \mu(p-1)$

else

$a \leftarrow y + \mu(p-2)x^{p-1}$

$b \leftarrow 1 + \mu(p-1)x^{p-2}$

end if

$x \leftarrow a/b$

until convergence

return x

3 Maximizing dual objective via Newton ascent ($p > 1$)

From Section 2.4.1, we see that it suffices to consider the case $p > 2$ for convex norm balls. Then Slater's condition holds and strong duality implies that solving (D) is equivalent to (P). From Section 2.4.2 we see that function $z_p(y)$, implicitly defined as $0 = z_p(y) - y + [z_p(y)]^{p-1}$, is continuously differentiable in y , even for $p > 2$. Observe that in the latter case $\text{prox}_{s_p}(y) = z_p(y)$. Letting x be non-negative without loss of generality, we may rewrite

$$\begin{aligned} f_\mu(x; y) &= \mu^{2/(2-p)} \left[\frac{1}{2} \left(\frac{y}{\mu^{1/(2-p)}} - \frac{x}{\mu^{1/(2-p)}} \right)^2 + \frac{1}{p} \left(\frac{x}{\mu^{1/(2-p)}} \right)^p \right] \\ &= \mu^{2/(2-p)} f_1(\tilde{x}; \tilde{y}), \quad \text{where } \tilde{x} = x/\mu^{1/(2-p)}, \tilde{y} = y/\mu^{1/(2-p)}, \end{aligned}$$

which asserts that

$$\text{prox}_{\mu s_p}(y) = \mu^{1/(2-p)} \text{prox}_{s_p}(y/\mu^{1/(2-p)}). \quad (10)$$

Thus $x_i^*(\mu) = \text{prox}_{\mu s_p}(y_i) = \mu^{1/(2-p)} z_p(y_i/\mu^{1/(2-p)}) > 0$ is a continuously differentiable function of μ , with derivative

$$x_i^{*'}(\mu) = -\frac{x_i^*(\mu)^{p-1}}{1 + \mu(p-1)x_i^*(\mu)^{p-2}} \quad (11)$$

obtained by applying the implicit function differentiation rule to equation (4). It follows immediately that $x_i^*(\mu)$ is strictly decreasing in μ and satisfies

$$0 < x_i^*(\|\mathbf{y}\|_q) \leq x_i^*(\mu) \leq x_i^*(0) = y_i$$

on the interval $[0, \|\mathbf{y}\|_q]$. Expressions (4) and (11) also allow one to derive formulas for the derivatives of the dual objective g in (3) and verify that it is twice continuously differentiable:

$$g'(\mu) = \frac{1}{p} \sum_{i=1}^d x_i^*(\mu)^p - \frac{1}{p} = \frac{1}{p} (\|\mathbf{x}^*(\mu)\|_p^p - 1), \quad (12)$$

$$g''(\mu) = \sum_{i=1}^d x_i^*(\mu)^{p-1} x_i^{*\prime}(\mu) = - \sum_{i=1}^d \frac{x_i^*(\mu)^{2p-2}}{1 + \mu(p-1)x_i^*(\mu)^{p-2}}, \quad (13)$$

where (12) is due to Danskin's theorem; see, e.g., Bertsekas (1999, Proposition B.25) or Lange (2016, Proposition 3.2.6).

Thus the dual problem (D) can be solved efficiently by a Newton method with backtracking

$$\mu_{n+1} = \mu_n - t_n \frac{g'(\mu_n)}{g''(\mu_n)}, \quad (14)$$

where the step size $t_n \in (0, 1]$ ensuring the ascent property can be found by the Armijo rule. Since $\lim_{\mu \rightarrow 0^+} x_i^*(\mu) = x_i^*(0) = y_i$, the directional derivative of g at 0 toward the positive direction is $\frac{1}{p}(\|\mathbf{y}\|_p^p - 1) > 0$. Also recall that the solution μ^* to the dual (D) lies in $(0, \|\mathbf{y}\|_q]$ as demonstrated in Section 2.3. Any initial point in this interval ensures all iterates remain in $(0, \|\mathbf{y}\|_q]$ by the ascent property of iteration (14). The development so far is summarized in Algorithm 2.

The following proposition establishes quadratic convergence of Algorithm 2 and shows that backtracking is not needed after a few steps:

Proposition 2 *The Newton iterates $\{\mu_k\}$ generated by Algorithm 2 converge quadratically to the solution μ^* to (D) after a number of backtracks less than or equal to*

$$\frac{M^2 L^2 / m^5}{\alpha \beta \min\{1, 9(1 - 2\alpha)^2\}} (g(\mu^*) - g(\mu_0)), \quad (15)$$

where

$$M = \|\mathbf{y}\|_{2p-2}^{2p-2}, \quad m = \sum_{i=1}^d \frac{[x_i^*(\|\mathbf{y}\|_q)]^{2p-2}}{1 + \|\mathbf{y}\|_q (p-1) y_i^{p-2}}, \quad \text{and}$$

$$L = (p-1) \sum_{i=1}^d [2M_i + \|\mathbf{y}\|_q N_i], \quad q = p/(p-1), \quad \text{with}$$

$$M_i = \max\{x_i^*(\|\mathbf{y}\|_q)^{3p-4}, y_i^{3p-4}\}, \quad N_i = \max\{x_i^*(\|\mathbf{y}\|_q)^{3p-6}, y_i^{3p-6}\}.$$

Proof 1 For a twice continuously differentiable and strongly convex objective function with a Lipschitz continuous Hessian, convergence of Newton's method is quadratic after a limited number of backtracks (Boyd and Vandenberghe, 2004, §9.5.3). Thus it suffices to show that $g(\mu)$ in (3) satisfies these conditions.

We establish a negative upper bound on $g''(\mu)$ and a finite upper bound on the magnitude of the third derivative $|g'''(\mu)|$. The second expression for $g''(\mu)$ in (13) and that $0 < x_i^*(\|\mathbf{y}\|_q) \leq x_i^*(\mu) \leq y_i$ for $\mu \in [0, \|\mathbf{y}\|_q]$ make clear

$$\sum_{i=1}^d \frac{[x_i^*(\|\mathbf{y}\|_q)]^{2p-2}}{1 + \|\mathbf{y}\|_q(p-1)y_i^{p-2}} = m \leq -g''(\mu) \leq M = \|\mathbf{y}\|_{2p-2}^{2p-2}$$

in this interval, since $x_i^*(\|\mathbf{y}\|_q) = \text{prox}_{\|\mathbf{y}\|_q, s_p}(y_i)$.

To see that $g(\mu)$ is three times continuously differentiable, note that $x_i^*(\mu)$ is twice continuously differentiable with second derivative

$$x_i^{*''}(\mu) = -\frac{(p-1)[x_i^*(\mu)^{p-2} + \mu x_i^*(\mu)^{2p-4}]}{[1 + \mu(p-1)x_i^*(\mu)^{p-2}]^2} x_i^{*'}(\mu).$$

Equation (11) further implies that $x_i^{*''}(\mu)$ is also bounded on the interval, so that

$$g'''(\mu) = \sum_{i=1}^d [(p-1)x_i^*(\mu)^{p-2} x_i^{*'}(\mu)^2 + x_i^*(\mu)^{p-1} x_i^{*''}(\mu)]$$

is well-defined, and $|g'''(\mu)| \leq (p-1) \sum_{i=1}^d [2M_i + \|\mathbf{y}\|_q N_i] = L$.

Expression (15) follows from (Boyd and Vandenberghe, 2004, Eq. (9.40)). \square

Numerical consideration A simple numerical device greatly improves the stability of Algorithm 2. In computing the Newton step in iteration (14), overflow may occur when $|x_i^*(\mu)|^p$ becomes too large. This phenomenon is prominent, of course, when p is large. A remedy is to use $(|x_i^*(\mu)|/\max_j |x_j^*(\mu)|)^p$ to normalize the first (12) and second (13) derivatives of $g(\mu)$ when $(\max_j |x_j^*(\mu)|)^p$ is too large, say, greater than 10^{10} .

4 Maximizing dual objective via bisection

Solutions when $p \in (0, 1)$ are hindered by the lack of convexity of the unit ball. When $p > 1$, bisection offers a slower alternative to the Newton methods for finding the root of $g'(\mu)$, the derivative of the dual objective function $g(\mu)$ in problem (D). The last expression in equation (12) shows that bisection on $g'(\mu)$ is equivalent to that on the norm function $\|\mathbf{x}^*(\mu)\|_p$. This function is continuously monotone decreasing, and we simply need to find the μ that corresponds to $\|\mathbf{x}^*(\mu)\|_p = 1$. For $p < 1$, the delicacy lies in that solution sets $P_{B_p}(\mathbf{y})$ and the associated $\mathbf{x}^*(\mu)$ can be multi-valued. Further, the dual function $g(\mu)$ is no longer smooth.

Fortunately, $g(\mu)$ is concave and single-valued even if $\mathbf{x}^*(\mu)$ is multi-valued, so that $g(\mu)$ always has well-defined directional derivatives. For concreteness, we define the radius function

$$r(\mu) = \max_{\mathbf{x}} \{\|\mathbf{x}^*(\mu)\|_p : \mathbf{x}^*(\mu) \in \text{argmin}_{\mathbf{x}} \mathcal{L}(\mathbf{x}, \mu)\}. \quad (16)$$

It will be also convenient to define the maximum proximal operator of μs_p :

$$\max \operatorname{prox}_{\mu s_p}(y) = \max\{u : u \in \operatorname{prox}_{\mu s_p}(y)\}.$$

Recall that $z_p(y)$ is the root of $0 = z - y + z^{p-1}$ greater than m_p . Since $z_p(y) > m_p$, the function $\max \operatorname{prox}_{s_p}(y)$ is single-valued and right-continuous. It takes a jump of size κ_p at $y = r_p$, and is strictly increasing from there. On the other hand, from relation (10) and Proposition 1, the map $\mu \mapsto \max \operatorname{prox}_{\mu s_p}(y)$ when $\mu > 0$ and $y > 0$ is held fixed is decreasing and left-continuous, with a discontinuity only at $\mu = (y/r_p)^{2-p}$, before which it is strictly decreasing on $(0, (y/r_p)^{2-p})$.

Since $\mathbf{x}^*(\mu) = (x_1^*(\mu), \dots, x_d^*(\mu))$ and $x_i^*(\mu) = \operatorname{prox}_{\mu s_p}(y_i)$, as μ tends to ∞ from 0, $r(\mu)$ monotonically decreases from $\|\mathbf{y}\|_p$ down to 0, and is left-continuous. Let $\bar{\mu}$ denote a discontinuity in $\mathbf{x}^*(\mu)$. Each $x_i^*(\mu)$, and in turn $g(\mu)$, is single-valued and differentiable both at $\bar{\mu} - \epsilon$ and $\bar{\mu} + \epsilon$ for sufficiently small $\epsilon > 0$. Therefore, the subdifferential satisfies

$$\partial g(\bar{\mu}) = \left[\left(\lim_{\epsilon \downarrow 0} r(\bar{\mu} + \epsilon) - 1 \right) / p, \left(\lim_{\epsilon \downarrow 0} r(\bar{\mu} - \epsilon) - 1 \right) / p \right],$$

and we see that the inclusion $1 \in [\lim_{\epsilon \downarrow 0} r(\mu + \epsilon), \lim_{\epsilon \downarrow 0} r(\mu - \epsilon)]$ is necessary and sufficient for maximizing $g(\mu)$. Bisection is therefore guaranteed to return a sufficiently small interval $[\mu - \delta, \mu + \delta]$ such that $1 \in [r(\mu + \delta), r(\mu - \delta)]$ for any $\delta > 0$.

As strong duality is no longer guaranteed, a final remaining concern is the possibility of nonzero duality gap. The following proposition shows that this possibility is rare.

Proposition 3 *Let $\omega = \inf\{\mu : r(\mu) \leq 1\}$. Suppose $1 \in \nu(\omega)$ for the multi-valued norm function $\nu(\mu) = \{\|\mathbf{x}^*\|_p : \mathbf{x}^* \in \operatorname{argmin}_{\mathbf{x}} \mathcal{L}(\mathbf{x}, \mu)\}$. Then the point $\mathbf{x}^*(\omega) \in \operatorname{argmin}_{\mathbf{x}} \mathcal{L}(\mathbf{x}, \omega)$ with $\|\mathbf{x}^*(\omega)\|_p = 1$ solves (P).*

Proof 2 *Recall $\|\mathbf{x}^*(\omega)\|_p = 1$. For any \mathbf{x} satisfying $\|\mathbf{x}\|_p \leq 1$, we have*

$$g(\omega) = \mathcal{L}[\mathbf{x}^*(\omega), \omega] = \frac{1}{2} \|\mathbf{y} - \mathbf{x}^*(\omega)\|_2^2 \leq \mathcal{L}(\mathbf{x}, \omega) \leq \frac{1}{2} \|\mathbf{y} - \mathbf{x}\|_2^2.$$

Hence, $\mathbf{x}^(\omega) \in P_{B_p}(\mathbf{y})$ and the duality gap is zero.*

Bisection can thus be understood as finding the ω defined in this proposition. If $r(\omega) = 1$, then the projection problem is solved. Assuming $r(\omega) < 1$ contradicts the left-continuity of $r(\mu)$ and the definition of ω . Hence, $r(\omega) > 1$ and $r(\omega + \epsilon) < 1$. Repeating the argument of Proposition 3 yields the estimate

$$\frac{1}{2} \|\mathbf{y} - \mathbf{x}^*(\omega)\|_2^2 + \frac{r(\omega)^p - 1}{p} \leq \frac{1}{2} \|\mathbf{y} - \mathbf{x}\|_2^2$$

for all $\mathbf{x} \in P_{B_p}(\mathbf{y})$. Thus a small gap $r(\omega) - 1$ implies a good approximation to a projected point—this is what we find in practice. Algorithm 3 provides pseudocode for the bisection method.

5 Related work

5.1 Double bisection method for $p > 1$

In Liu and Ye (2010), the $\ell_{1,q}$ proximal problem arising from $\ell_{1,p}$ multitask learning ($p > 1, 1/p + 1/q = 1$) is studied:

$$\min_{\mathbf{Z} \in \mathbb{R}^{d \times s}} \frac{1}{2} \|\mathbf{Z} - \mathbf{V}\|_2^2 + r \sum_{i=1}^s \|\mathbf{z}_i\|_q,$$

where \mathbf{z}_i is the i th column of matrix \mathbf{Z} . Note that this splits into s independent evaluations of the proximal operator $\text{prox}_{r\|\cdot\|_q}(\mathbf{y})$ for solving (F). If $\mathbf{y} > \mathbf{0}$ and $r = 1$, the optimal solution \mathbf{z}^* to (F) satisfies the stationary condition

$$\mathbf{z}^* - \mathbf{y} + \|\mathbf{z}^*\|_q^{1-q} \mathbf{z}^{*(q-1)} = \mathbf{0}, \quad (17)$$

where $\mathbf{u} = \mathbf{x}^{(q-1)}$ is defined elementwise by $u_i = \text{sgn}(x_i)|x_i|^{q-1}$.

The value of the optimal multiplier $c^* = \|\mathbf{z}^*\|_q^{1-q}$ is unknown, so it is proposed to determine c^* by finding the root to the auxiliary function

$$\phi(c) = \psi(c) - c, \quad c \geq 0, \quad (18)$$

where $\psi(c) = [\sum_{i=1}^n (\omega_i^{-1}(c))^q]^{\frac{1-q}{q}}$ with $\omega_i(z) = \frac{y_i - z}{z^{q-1}}, 0 < z \leq y_i$. It is shown that $\phi(c)$ has a unique root in $[\min_{i=1, \dots, d} \gamma_i, \max_{i=1, \dots, d} \gamma_i]$ where

$$\gamma_i = \frac{1 - \epsilon}{\epsilon^{q-1} y_i^{q-2}}, \quad \epsilon = \frac{\|\mathbf{y}\|_{p-1}}{\|\mathbf{y}\|_p} \in (0, 1). \quad (19)$$

Hence its root is found by bisection. Evaluation of $\phi(c)$ requires inversion of the third auxiliary function $\omega_i(z)$ for each i , which is accomplished by finding the root of yet another auxiliary, monotone function

$$h_c^{y_i}(z) = z - y + cz^{q-1} \quad (20)$$

by bisection. This constitutes a nested or double bisection algorithm.

For $p > 1$, it is now clear that the root of the auxiliary function (20) of Liu and Ye (2010) is equivalent to equation (4) with substitution $p \leftarrow q$ and $\mu \leftarrow c$, i.e., $\text{prox}_{cs_q}(y_i)$. Thus we have also shown that at least one of the nested bisection routines for solving (F) Liu and Ye (2010) can be replaced by the faster Newton method (Algorithm 1). The other root finding of the more esoteric auxiliary function $\phi(c)$ is related to solving

$$\|\mathbf{y} - c^2 \mathbf{x}^*(c^{1-p})\|_q^{1-q} = c$$

via Moreau's identity,

$$\text{prox}_{cs_q}(y_i) = y_i - c \text{prox}_{c^{-1}s_p}(y_i/c) = y_i - c^2 x_i^*(c^{1-p}).$$

In solving this equation via bisection, the interval (19) involves both $1/y_i^{q-2}$ and $(\|\mathbf{y}\|_p - 1)/\|\mathbf{y}\|_p$, so when p is large (q is close to 1), initial values may run into numerical difficulties. In contrast, our more transparent approach solves the dual optimality condition $g'(\mu) = 0$ for (D), or equation

$$\|\mathbf{x}^*(\mu)\|_p^p = 1, \quad (21)$$

in the straightforward interval $[0, \|\mathbf{y}\|_p]$. The left hand side is twice continuously differentiable with respect to μ , and so Newton’s method (Algorithm 2) efficiently solves this equation. So when $p > 1$, our approach constitutes a “double Newton” method. If $p < 1$, the outer Newton is replaced with bisection; the inner Newton for $\text{prox}_{s_p}(\cdot)$ remains intact.

5.2 Projected Newton for $p > 1$

Assuming again $\mathbf{y} > \mathbf{0}$ and $r = 1$ without loss of generality, Barbero and Sra (2018) proposes to solve (F) together with a redundant constraint $\mathbf{z} \geq \mathbf{0}$ using projected Newton (Bertsekas, 1982). Let \tilde{g} denote the objective of (F). An inactive component of \mathbf{z} is defined as the i th component with either $z_i > 0$ or $z_i = 0$ but $\nabla_i \tilde{g}(\mathbf{z}) < 0$. If we denote the set of these by I , \tilde{g} is differentiable within I :

$$\begin{aligned} \nabla_I \tilde{g}(\mathbf{z}) &= \mathbf{z}_I - \mathbf{y}_I + \bar{\mathbf{z}}_I, & \bar{\mathbf{z}} &= (\mathbf{z}/\|\mathbf{z}\|_q)^{q-1}, \\ \nabla_I^2 \tilde{g}(\mathbf{z}) &= \text{diag}(\mathbf{v}_I) + c \bar{\mathbf{z}}_I \bar{\mathbf{z}}_I^T, & \mathbf{v} &= \mathbf{1} - c(\mathbf{z}/\|\mathbf{z}\|_q)^{q-2}, \quad c = (1-p)\|\mathbf{z}\|_q^{-1}, \end{aligned} \quad (22)$$

where ∇_I and ∇_I^2 denote the gradient and Hessian restricted within I , respectively, and \mathbf{v}_I refers to the subvector of \mathbf{v} indexed by I . The Newton update of inactive components \mathbf{z}_I is then projected onto the nonnegative orthant:

$$\mathbf{z}_I := \left[\mathbf{z}_I - t \left(\mathbf{v}_I^{-1} \odot \nabla_I g(\mathbf{z}) - \frac{(\mathbf{v}_I^{-1} \odot \bar{\mathbf{z}}_I)(\mathbf{v}_I^{-1} \odot \bar{\mathbf{z}}_I)^T \nabla_I g(\mathbf{z})}{1/c + \bar{\mathbf{z}}_I^T (\mathbf{v}_I^{-1} \odot \bar{\mathbf{z}}_I)} \right) \right]_+, \quad (23)$$

where $(\cdot)^{-1}$ and \odot denote elementwise inverse and multiplication, respectively; $[\mathbf{x}]_+ = \max(\mathbf{x}, \mathbf{0})$ componentwise. The step size t is chosen by using a backtracking line search.

Per-iteration complexity of the projected Newton method (23) is lower than the univariate dual method (14), since the latter requires Algorithm 1 internally to evaluate $x_i^*(\mu)$. However, the construction of the restricted Hessian (22) indicates that the curvature of the objective of (F) near the boundary ($\mathbf{z} = \mathbf{0}$) can become extreme. This suggests numerical instability and possible overflows. The reference implementation³ by the authors of Barbero and Sra (2018) faces this problem by adding several *ad hoc* safeguards, including a switch to gradient descent. Despite this, we encountered numerical inaccuracies using projected Newton in our experiments under large values of p ; see Section 6.

³Available at <https://github.com/albarji/proxTV/blob/master/src/LPopt.cpp>

5.3 Bisection method of Chen et al. (Chen et al., 2021) for $p < 1$

A referee pointed out potential similarities between the work of Chen, Jiang, and Liu (Chen et al., 2021) and our univariate dual method. As a subproblem of a low-rank matrix decomposition problem, Chen et al. (2021, Sect. IV-A) considers problem (P) and arrives at equation (21) via the Karush–Kuhn–Tucker (KKT) conditions derived from the Lagrangian of the reformulated primal (P''). This work also suggests finding the root of equation (21) by bisection. Regarding the associated proximal map $\text{prox}_{\mu s_p}(y_i)$ for $p < 1$, Chen et al. (2021) considers equation (4) directly from the KKT conditions. Since finding the root of equation (4) alone is not sufficient for fully evaluating $\text{prox}_{\mu s_p}(y_i)$, an additional heuristic is developed Chen et al. (2021, Theorems 3 and 4).

While close to our approach, the work of Chen et al. ignores that solving (21) is in fact equivalent to solving the dual (D). As a result, Chen et al. (2021) fails to capitalize that an (outer) Newton method can be employed to yield much faster convergence for $p > 1$ (see Proposition 2), while on the other hand when $p < 1$, misses discontinuity of the target function $g'(\mu)$ as well as the possibility of nonzero duality gap. Our inspection of the dual problem (D) also brings focus to the map $\text{prox}_{\mu s_p}(\cdot)$, which is well-studied for $p < 1$ and more principled than solely analyzing equation (4). In fact, Theorems 3 and 4 of Chen et al. (2021) are subsumed by Proposition 1 due to Marjanovic and Solo (2012), which predates Chen et al. (2021) and our present paper by several years.

5.4 MM algorithms for $p < 1$

While this letter is under review, an iterative re-weighted ℓ_1 -ball projection (IRBP) algorithm has been posted online as a preprint (Yang et al., 2021). The main idea behind the IRBP algorithm is to “smooth” the nonconvex unit ℓ_p norm ball $B_p = \{\mathbf{x} = (x_1, \dots, x_d) : \sum_{i=1}^d |x_i|^p \leq 1\}$ by

$$B_{p,\epsilon} = \{\mathbf{x} : \sum_{i=1}^d |x_i + \epsilon_i|^p \leq 1\}$$

for $\epsilon = (\epsilon_1, \dots, \epsilon_d) > \mathbf{0}$ (recall that we set $r = 1$), and iteratively relax $B_{p,\epsilon}$ by a weighted ℓ_1 norm ball

$$r_n B_{1,w_n} = \{\mathbf{x} : \sum_{i=1}^d w_{n,i} |x_i| \leq r_n\}$$

for the n -th iterate $\mathbf{x}_n = (x_{n,1}, \dots, x_{n,d})$. Here $r_n = 1 - \sum_{i=1}^d (x_{n,i} + \epsilon_i)^p + \sum_{i=1}^d w_{n,i} |x_{n,i}|$ and $w_{n,i} = p(|x_{n,i}| + \epsilon_i)^{p-1}$. The next iterate is obtained by minimizing $f_0(\mathbf{x}) = \frac{1}{2} \|\mathbf{x} - \mathbf{y}\|_2^2$ on $r_n B_{1,w_n}$, which can be efficiently solved by a trivial modification of (unweighted) ℓ_1 -ball projection algorithms, e.g., (Duchi et al., 2008; Condat, 2016). The authors of Yang et al. (2021) show that, for a certain dynamic update strategy for ϵ , every cluster point of the iterate $\{\mathbf{x}_n\}$ is a stationary point of problem (P).

We note that IRBP is an instance of majorization-minimization (MM) algorithms (Lange, 2016). With the smoothed ℓ_p norm ball we aim to minimize $f_\epsilon(\mathbf{x}) \triangleq f_0(\mathbf{x}) + \iota_{B_{p,\epsilon}}(\mathbf{x})$, which is a perturbed objective for the unconstrained problem (P') that is equivalent to the original problem (P). For each iterate \mathbf{x}_n , the surrogate function

$$g(\mathbf{x}|\mathbf{x}_n) = f_0(\mathbf{x}) + \iota_{r_n B_{1,w_n}}(\mathbf{x})$$

majorizes $f_\epsilon(\mathbf{x})$ at \mathbf{x}_n , i.e., $g(\mathbf{x}|\mathbf{x}_n) \geq f_\epsilon(\mathbf{x})$ for all \mathbf{x} and $g(\mathbf{x}_n|\mathbf{x}_n) = f_\epsilon(\mathbf{x}_n)$, since $r_n B_{1,w_n} \subset B_{p,\epsilon}$ and $\iota_{B_{p,\epsilon}}(\mathbf{x}_n) = \iota_{r_n B_{1,w_n}}(\mathbf{x}_n) = 0$. By iteratively minimizing the surrogate function and driving $\epsilon \downarrow \mathbf{0}$, the unperturbed problem (P) is expected to be solved.

IRBP is a primal algorithm as opposed to our dual bisection algorithm. With a proper scheduling for driving the ϵ down to zero, IRBP converges to a feasible stationary point of the primal (P) from any feasible initial point. Optimality of the convergent stationary point depends on the choice of the initial point. On the other hand, since the dual objective $g(\mu)$ is concave, the dual bisection method can find the dual optimum from any initial point. If the duality gap is zero, or equivalently the root of (21) exists, then the the primal optimum is found (Proposition 3). However, if the duality gap is positive or $g'(\mu) - 1$ has a sign-changing discontinuity, then the primal solution recovered from the dual optimum may not even be feasible, contrary to IRBP. Although we have found that this possibility is rare in practice (see the next section), examples exhibiting nonzero duality gap do exist (see Example 5.1 of Yang et al. (2021)). In this case, rescaling the primal solution by its ℓ_p norm results in a feasible point. Although there is no guarantee that the stationary conditions are met, our experience tells that this rescaling often yields satisfactorily small primal objective values.

6 Empirical results

6.1 Multi-task learning

Our empirical assessment of the proposed methods begins with an application to multi-task learning under $\ell_{1,p}$ regularization. Let $\mathbf{A} \in \mathbb{R}^{m \times d}$ be a design matrix containing data with feature dimension d , and $\mathbf{Y} \in \mathbb{R}^{m \times k}$ be the matrix of response variables, where the columns are observations corresponding to k tasks. We seek the matrix $\mathbf{B} \in \mathbb{R}^{d \times k}$ with rows denoted $\mathbf{B}_{(i,\cdot)}$ as the solution to

$$\operatorname{argmin}_{\mathbf{B} \in \mathbb{R}^{d \times k}} \frac{1}{2} \|\mathbf{A}\mathbf{B} - \mathbf{Y}\|_F^2 + \tau \sum_{i=1}^d \|\mathbf{B}_{(i,\cdot)}\|_p. \quad (24)$$

The second term promotes row-wise sparsity by way of an $\ell_{1,p}$ norm, and coincides with the usual group lasso when $p = 2$. Zhang et al. (2010) motivates other choices of p implying different “group discounts” to the loss, showing that proper choice of $p \in (1, \infty] \setminus \{2, \infty\}$ can significantly improve performance. Liu and Ye (2010) confirms this finding and develops a more efficient double-bisection algorithm mentioned above. This is used to evaluate proximal maps for $\ell_{1,p}$ norms in the popular package SLEP

Liu et al. (2011), and more recently by Sra (2012), Vogt and Roth (2012), and Zhou et al. (2015) within a proximal gradient algorithm for fitting (24).

Following the data generation in Zhou et al. (2015), we show that replacing double-bisection by our dual Newton ascent (Algorithm 2) reduces runtime by orders of magnitude. We draw entries of the covariate matrix \mathbf{A} as standard Gaussians shifted to have mean 2. We choose 10 rows (groups) of the true d -by- k coefficient matrix \mathbf{B}^* to be nonzero, drawn as standard Gaussian vectors. Then $\mathbf{Y} = \mathbf{A}\mathbf{B}^* + \mathbf{Z}$ where entries of \mathbf{Z} are independent zero mean Gaussian with standard deviation 0.1. The projection tolerances for all instances in the multi-task learning example are set to 10^{-6} , with iteration limit 5000 per projection step. We note that for $p \approx 5$ and above, the double bisection approach reaches the maximum iteration limit in many instances. We focus on efficiency as all methods run within the same outer proximal gradient algorithm, and reach identical solutions up to specified relative tolerance criterion of 10^{-3} . Due to runtime considerations of the competing method, we fix τ at a constant that scales with the product of $d \times p$ rather than choose by cross-validation for each trial. Our algorithm and the competing method are initialized at identical starting value, obtained by adding another standard Gaussian to the true solution. The proximal gradient step size is set to $1/2$ divided by the largest eigenvalue of $\mathbf{A}^T \mathbf{A}$.

Fig. 1 shows that as curvature increases with p , the method of Liu and Ye (2010) struggles even at small scales, while our method consistently terminates in a fraction of a second. Methods are run under matched relative tolerance and reach identical solutions at convergence. The right panel shows that our algorithm remains tractable when the dimension times the number of tasks reaches millions, converging in several minutes consistently over a wide range of choices p .

6.2 High-dimensional projections

Inspired by their success in the context of multi-task learning, we now examine the runtime, accuracy, and scalability of the proposed methods more closely. We consider projecting onto ℓ_p balls in dimension $d = 1,000,000$. Having already established the limitations of the double-bisection method, we compare our dual Newton ascent and bisection methods to the projected Newton (Barbero and Sra, 2018) for $p > 1$, and to the IRBP method (Yang et al., 2021, Algorithm 1) for $p < 1$. Since the IRBP method involves a crucial subproblem of projection onto a weighted ℓ_1 ball, we employ three implementations of weighted ℓ_1 -ball projection:

- IRBP1: weighted version of Condat’s algorithm (Condat, 2016), in which catastrophic cancellation is avoided at the expense of computational complexity;
- IRBP2: weighted version of Duchi et al’s algorithm (Duchi et al., 2008);
- IRBP3: reference implementation by the authors of Yang et al. (2021),⁴ which employs an alternating projection method.

Additionally, a naïve method making use of the nearest available exact projection, choosing the ℓ_∞ ball for $p \in (4, \infty)$, the ℓ_2 ball for $p \in (\frac{3}{2}, 4]$, the ℓ_1 ball for $p \in (\frac{1}{2}, \frac{3}{2}]$,

⁴Available at <https://github.com/Optimizater/Lp-ball-Projection>

and the ℓ_0 ball for $p \in (0, \frac{1}{2}]$ is compared; these nearest exact projections are then scaled to observe the ℓ_p -ball constraint.

Convergence of the algorithms are declared as follows. For the dual Newton ascent (Algorithm 2), convergence is declared when the distance $\text{obj}_n = \|\mathbf{y} - \mathbf{x}_n\|_2$ of the current iterate \mathbf{x}_n to \mathbf{y} satisfied the inequality

$$|\text{obj}_n - \text{obj}_{n-1}| < 10^{-12}(1 + \text{obj}_{n-1}).$$

For bisection, Algorithm 3 is run until $\mu_r - \mu_l < 10^{-12}$ and either of the following criteria is met:

$$r(\mu_l) - r(\mu_r) < 10^{-7}(1 + r(\mu_l)) \quad \text{or} \quad \mu_r - \mu_l < \epsilon_{\text{mach}}\mu_r,$$

where $\epsilon_{\text{mach}} \approx 2.22 \times 10^{-16}$ is the machine epsilon. These criteria are needed to cope with the discontinuity of the function $r(\mu)$. The convergence criteria for the projected Newton (Barbero and Sra, 2018) and IRBP Yang et al. (2021) follow the reference implementations, whose URLs are provided in the footnotes at the end of Section 3 and in this subsection.

All the simulations were run on a Linux machine with an Intel Xeon E5-2650 v4 CPU @ 2.20GHz with 12 cores. A single core was used for each value of the power p . The code was written in the Julia programming language, except the projected Newton for which the compiled C++ reference implementation was directly called from Julia, and IRBP3 for which the reference implementation in Python was called via `PyCall.jl`.⁵

Results under several performance measures are reported in Tables 1 and 2. The components of each exterior point to be projected, \mathbf{y} , were sampled as independent standard normal entries. The radius r of the ℓ_p ball for a given \mathbf{y} was chosen uniformly from $(0, \|\mathbf{y}\|_p)$. All performance measures for a given p and method represent averages over 100 independent trials. The range of powers p considered are designed to elicit both typical and extreme behavior. Runtime is assessed via number of iterations as well as elapsed time in seconds until convergence. Since the radius r varies widely across the sampled external points, all the performance measures except runtime were computed after normalizing the coordinates, i.e., $x_i^* \leftarrow x_i^*/r$, $y_i \leftarrow y_i/r$, $i = 1, \dots, d$.

The objective value (“obj”) at convergence must be considered together with the KKT measures, defined as follows. The “KKT1” measure is the sum of absolute values of the right-hand side of equation (4) for $i = 1, \dots, d$:

$$\text{KKT1} = \sum_{i=1}^d |x_i^* - y_i + \mu^* |x_i^*|^{p-1} \text{sgn}(y_i)|. \quad (25)$$

The univariate dual methods (Algorithms 2 and 3) compute the dual optimal variable μ^* ; this measure can be directly calculated. However, other methods (naïve and projected Newton) do not generate this dual variable, and hence μ^* is estimated by the formula

$$\mu^* = (\mathbf{y}^T \mathbf{x}^* - \|\mathbf{x}^*\|_2^2) / \|\mathbf{x}^*\|_p^p$$

⁵Available at <https://github.com/JuliaPy/PyCall.jl>.

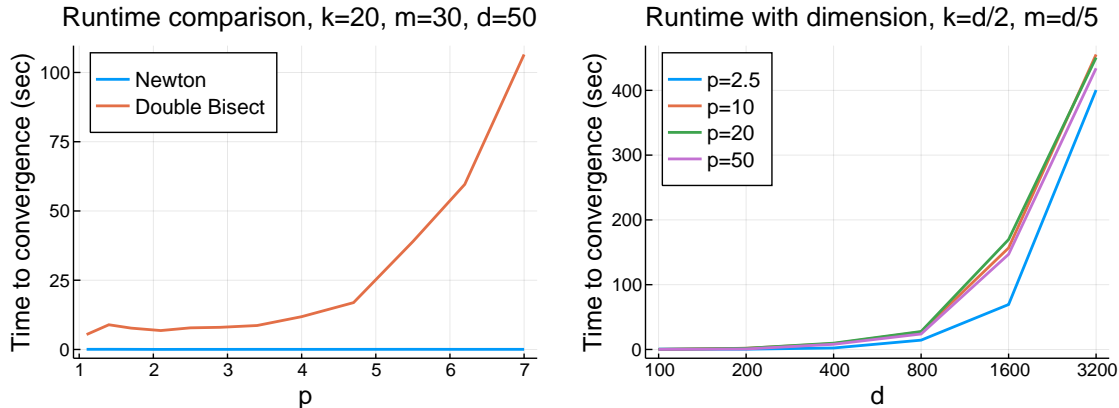


Figure 1: Prior method used in SLEP slows as p grows even on moderate problem size; our method scales to d, k in the thousands consistently over a wide range of p .

(see equation (5) in Section 2.3). This computed dual variable may be negative, but we nevertheless computed the KKT1 measure. If $|x_i^*|$ is very small (we used the threshold of 10^{-12}) but y_i is not, then $|x_i^*|^{p-1}$ is approximated by $|(\mu^*)^{-1}y_i|$ (see equation (7) in Section 2.4.1); this scenario is encountered usually when p is close to one. This correction is also valid for the non-convex case ($0 < p < 1$), in which equation (4) may not hold for every coordinate (see Remark 1 and Section 2.4.2).

It may be argued that KKT1 is favorable to the univariate methods, since the projected Newton solves a different dual problem (F). For this reason, another KKT measure (“KKT2”) quantifies the deviation from the optimality condition (17) of problem (F):

$$\text{KKT2} = \sum_{i=1}^d |z_i^* - y_i + (|z_i^*|/\|z^*\|_q)^{q-1} \text{sgn}(y_i)|, \quad q = \frac{p}{p-1},$$

which is valid only for $p \geq 1$, where $z^* = \mathbf{y} - \mathbf{x}^*$ is the computed optimal variable of problem (F). A similar numerical caution is warranted if $|z_i^*|$ is infinitesimally small, but this case usually occurs when q is close to one, or p is large. As a related measure, the ratio $\frac{1}{r}\|\mathbf{x}\|_p$ informs whether the projected point \mathbf{x} falls on the surface of the rB_p ; its difference from 1 measures the duality gap provided that the KKT measures are small (see the discussion below Proposition 3). All measures greater than 10^{10} are marked by ∞ .

For $p < 1$, instead of KKT2 we measure the duality gap

$$f_0(\mathbf{x}^*) - g(\mu^*).$$

If the μ^* in (25) is negative, then $x_i(\mu^*) = \text{prox}_{\mu^* s_p}(y_i)$ is undefined, hence we set $g(\mu^*) = \text{NaN}$ and count the number of trials yielding NaNs. Note that, if \mathbf{x}^* is infeasible, this metric may be misleading.

Our results in Table 1 indicate that over a wide range of $p > 1$, the dual Newton method successfully computes the projections with accuracy comparable to that of

bisection in a fraction of the runtime. The projected Newton is faster, which may be expected due to its C++ implementation as opposed to Julia. However, both KKT measures and constraint violation are at least an order of magnitude greater than dual Newton and bisection given similar numbers of iterations to converge, even though the KKT2 measure is favorable to this method by construction. In particular, the accuracy across all measures becomes noticeably worse as p increases, which is anticipated from the discussion in Section 3. For $p = 1.01$ and $p = 100$, the reference implementation of the projected Newton rounds them to $p = 1$ and $p = \infty$, respectively. The resulting accuracy, along with those of the naïve method, serves to illustrate the inadequacy of working only with computationally convenient projection operators.

The results for $p \in (0, 1)$ are presented in Table 2. Recall that in this non-convex setting, only bisection and IRBP are meaningful options. No rescaling for observing the ℓ_p -ball constraint is employed for either method. Nevertheless, the dual bisection method consistently delivered accurate projections for all the values of p tried, indeed with small duality gaps, supporting the theoretical finding in Proposition 3. The behavior of IRBP is a bit complicated. For $p \geq 0.5$ all three versions worked well with outcomes comparable to the dual bisection. (IRBP3 was excluded for $p = 0.5$ because it took more than two hours for each trial: 10134, 8358, 17031, 28022 seconds in the first four trials.) IRBP converged in fewer iterations than bisection when p is greater than 0.5, but constraint violation is at least an order of magnitude greater than bisection as well as the objective values; this is likely due to the convergence criteria, which followed the reference implementation (IRBP3). So, for this range of p , it appears that the two methods are comparable. For $p < 0.5$, however, both IRBP1 and IRBP3 tended to drive the iterates toward zero, while IRBP2 produced outputs that were the same as the inputs. For neither results we could not call for accuracy. Finally, it is interesting to note the performance of the naïve method when p is less than 0.5. The objective value was within 0.001% of bisection, while respecting the norm ball constraint. Not surprisingly, naïve solutions for this range of p were not dual feasible.

6.3 Compressed sensing

Having observed the effectiveness of the bisection approach for projection onto non-convex norm balls, in this section we consider its application to compressed sensing, i.e., recovery of a sparse signal from linear measurements. Suppose we want to estimate an unknown but sparse signal $\mathbf{s} \in \mathbb{R}^d$ from m noisy observations $\mathbf{b} \in \mathbb{R}^m$ through measurement or sensing matrix $\mathbf{A} \in \mathbb{R}^{m \times d}$ such that

$$\mathbf{b} = \mathbf{A}\mathbf{s} + \boldsymbol{\epsilon},$$

where $\boldsymbol{\epsilon} \in \mathbb{R}^m$ is the noise. A possible approach is to solve the ℓ_p -constrained least squares problem

$$\min_{\mathbf{x} \in \mathbb{R}^d} \frac{1}{2} \|\mathbf{b} - \mathbf{A}\mathbf{x}\|_2^2 \quad \text{subject to} \quad \|\mathbf{x}\|_p \leq r \quad (26)$$

for $p \in [0, 1]$. It is well known, especially when $p = 1$, that under certain conditions on the sensing matrix \mathbf{A} the solution \mathbf{x}^* to problem (26) is equal to \mathbf{s} with high probability (Donoho, 2006).

Table 1: Average performance of ℓ_p -ball projection algorithms for $d = 1,000,000$ ($p > 1$)

Method	p	Iters	Secs	KKT1	KKT2	Obj	$\frac{1}{n}\ \mathbf{x}^*\ _{p-1}$
Naive	1.01	1.000	0.1963	0.1390	2.053	503.593	-2.769e-15
Dual Newton	1.01	4.200	12.48	3.020e-9	1.663e-8	494.572	1.466e-8
Bisection	1.01	26.83	40.23	3.020e-9	3.725e-8	494.572	8.673e-10
Projected Newton	1.01	0.000	0.4648	0.1927	0.6943	544.706	-0.1164
Naive	1.05	1.000	0.1812	0.8063	2.946	563.572	4.741e-16
Dual Newton	1.05	4.120	11.99	1.187e-8	1.764e-8	447.537	9.759e-9
Bisection	1.05	26.66	39.28	1.188e-8	4.34e-8	447.537	-1.548e-9
Projected Newton	1.05	6.180	2.656	1.637e-6	1.305e-6	447.537	1.931e-8
Naive	1.1	1.000	0.1725	1.898	4.405	745.935	1.887e-17
Dual Newton	1.1	4.090	10.48	1.138e-7	1.617e-7	462.819	6.613e-8
Bisection	1.1	27.78	36.28	1.134e-7	2.962e-8	462.819	-1.961e-9
Projected Newton	1.1	5.410	2.366	9.094e-5	1.053e-6	462.819	2.115e-8
Naive	1.5	1.000	0.1614	10.42	38.50	1291.36	-1.588e-16
Dual Newton	1.5	4.050	8.065	5.065e-11	7.743e-7	502.465	9.42e-9
Bisection	1.5	36.66	31.62	5.061e-11	7.786e-10	502.465	1.946e-13
Projected Newton	1.5	4.220	1.936	0.03598	0.0001776	502.465	1.548e-7
Naive	4.0	1.000	0.1429	5.181e4	10740.0	517.692	-2.316e-15
Dual Newton	4.0	4.880	6.691	1.117e-10	6.446e-5	488.994	2.556e-9
Bisection	4.0	61.59	42.34	1.111e-10	3.132e-10	488.994	-1.36e-15
Projected Newton	4.0	6.420	2.476	0.01578	0.07242	488.993	1.232e-7
Naive	10.0	1.000	0.1444	8.506e5	119200.0	505.418	-2.421e-14
Dual Newton	10.0	6.870	13.41	7.165e-9	0.0003264	405.299	1.379e-9
Bisection	10.0	216.6	284.9	7.154e-9	4.595e-5	405.299	-2.359e-15
Projected Newton	10.0	10.77	3.931	0.1228	0.5518	405.299	1.398e-7
Naive	99.0	1.000	0.1475	2.318e6	4.908e5	248.933	4.453e-15
Dual Newton	99.0	12.03	12.78	4.423e-8	0.004281	225.815	4.045e-9
Bisection	99.0	218.5	208.7	4.431e-8	0.000912	225.815	4.796e-16
Projected Newton	99.0	13.18	3.775	0.1419	0.1335	225.814	1.563e-5
Naive	100.0	1.000	0.1459	8.748e5	5.165e5	221.562	-4.091e-15
Dual Newton	100.0	13.44	10.42	1.732e-8	0.001485	196.074	8.638e-10
Bisection	100.0	199.8	221.7	1.867e-8	0.0008292	196.074	-3.126e-15
Projected Newton	100.0	0.000	0.008133	1.32e12	1.8970e4	176.687	0.08643

Since the ℓ_1 -ball is the convex hull of the ℓ_0 -ball that exactly quantifies sparsity, use of ℓ_p norms with $p < 1$ is expected to recover \mathbf{s} better than ℓ_1 norm, as evidenced by Chartrand and Staneva (2008); Blumensath and Davies (2009); Chartrand and Yin (2016). Since in this case problem (26) is non-convex, its global optimum is difficult to find. However, the sequence generated by the projected gradient descent (PGD) method to approximately solve problem (26)

$$\mathbf{x}^{k+1} = P_{rB_p}[\mathbf{x}^k + \gamma_k \mathbf{A}^T(\mathbf{b} - \mathbf{A}\mathbf{x}^k)] \quad (27)$$

with $\mathbf{x}^0 = \mathbf{0}$ has been shown to perform well (Bahmani and Raj, 2013; Blumensath and Davies, 2009). Here $\gamma_k > 0$ is the step size at iteration k . Bahmani and Raj (Bahmani and Raj, 2013) analyzed the rate of convergence of \mathbf{x}^k to \mathbf{s} as a function of p , showing that the sufficient conditions for exact signal recovery become more stringent while robustness to noise and convergence rate worsen, as p increases from 0 to 1. Oymak et al. (Oymak et al., 2017; Sattar and Oymak, 2020) extended the analysis for more general (non-convex) constraint sets including ℓ_p -balls. Their experiments compared cases $p = 0, 0.5$, and 1, and suggest that while $p = 0$ outperforms $p = 1$, it is dominated by $p = 0.5$.

Our bisection approach for computing P_{rB_p} opens up the opportunity of fully assessing the performance of PGD (27) for various values of p . Following Oymak et al. (2017, Sect. III-A), we fix the dimension $d = 1000$ and vary the sparsity level s

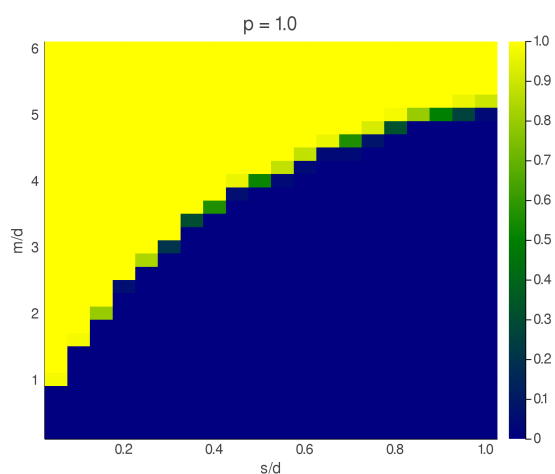
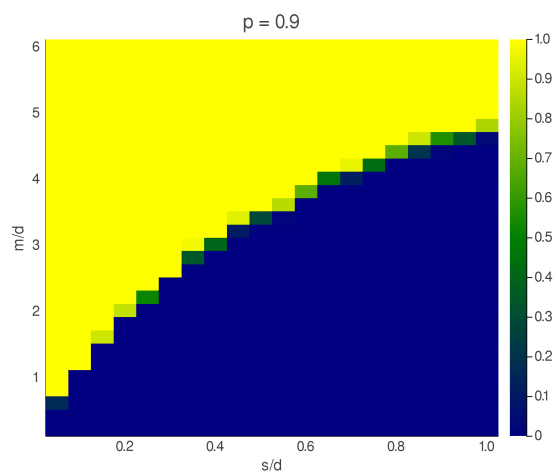
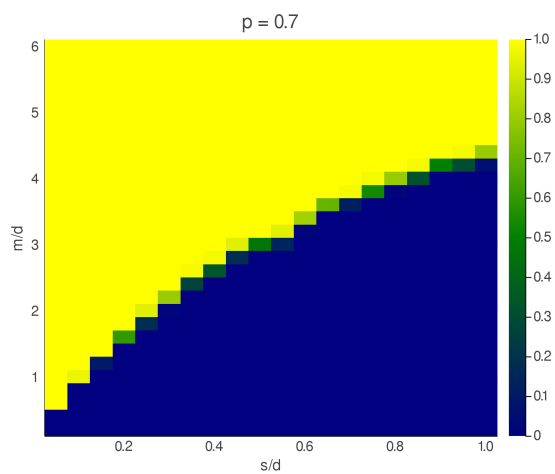
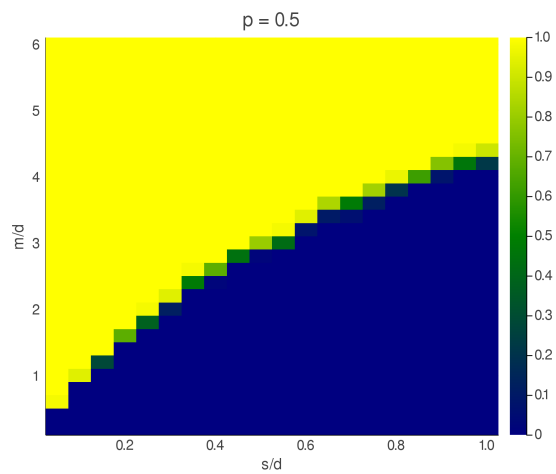
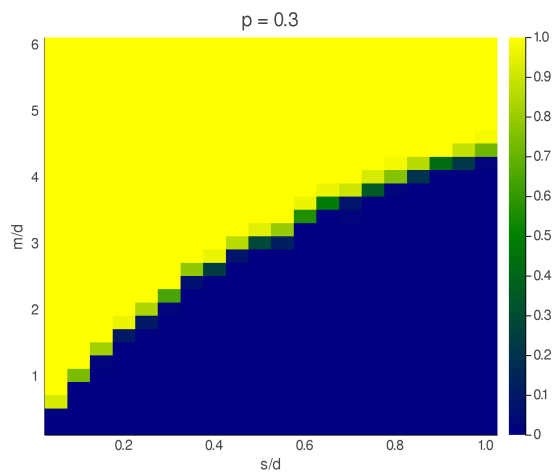
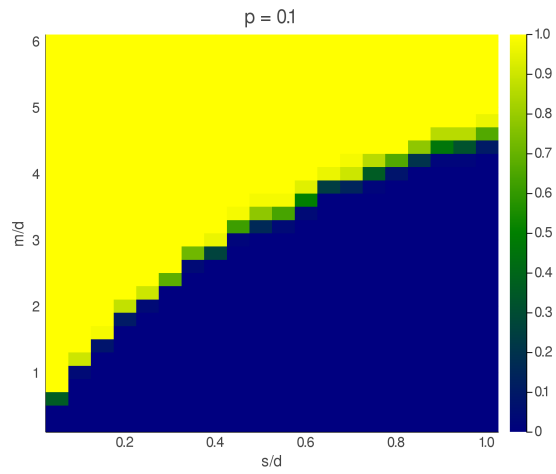
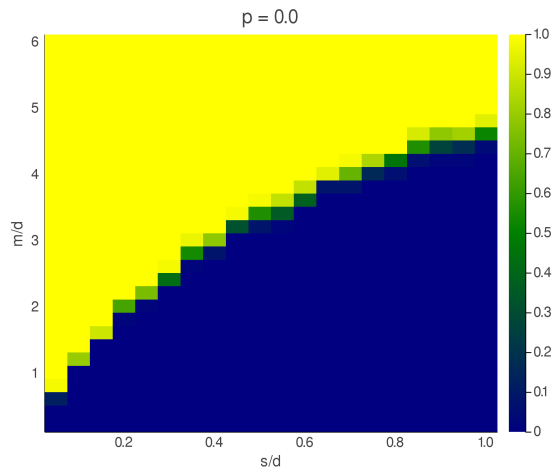
Table 2: Average performance of ℓ_p -ball projection algorithms for $d = 1,000,000$ ($p < 1$)

Method	p	Iters	Secs	KKT1	Duality gap	Obj	$\frac{1}{r} \ \mathbf{x}^*\ _{p-1}$	% NaN
Naive	0.1	1.0	0.49	0.0	NaN	34.24	3.611e-14	0
Bisection	0.1	243.9	43.64	0.0	4.874e-119	34.24	-4.147e-7	100
IRBP1	0.1	1001.0	198.6	0.0	NaN	999.9	-1.0	0
IRBP2	0.1	951.1	408.0	0.0	0.0	4.034e-14	5.686	100
IRBP3	0.1	1.0	4.641	0.0	NaN	999.9	-1.0	0
Naive	0.3	1.0	0.4496	0.0	NaN	157.7	-1.018e-14	0
Bisection	0.3	106.3	23.49	0.0	1.112e-38	157.7	-3.027e-8	100
IRBP1	0.3	1001.0	208.7	0.0	NaN	999.9	-1.0	0
IRBP2	0.3	1001.0	440.0	0.0	0.0	4.148e-14	5.686	100
IRBP3	0.3	1.0	5.742	0.0	NaN	999.9	-1.0	0
Naive	0.5	1.0	0.4509	4.541e-12	NaN	286.5	-6.459e-15	0
Bisection	0.5	77.04	19.17	9.371e-8	6.298e-22	281.7	4.692e-8	100
IRBP1	0.5	804.7	229.2	3.569e-14	4.328e-16	363.0	-0.02082	100
IRBP2	0.5	809.2	327.1	7.591e-13	4.335e-16	362.9	-0.02115	10
Naive	0.7	1.0	0.2217	0.0137	2.084e-9	762.3	3.197e-15	100
Bisection	0.7	52.3	20.94	1.73e-12	2.514e-15	365.1	-1.378e-8	100
IRBP1	0.7	8.37	2.355	1.428e-5	8.791e-10	417.4	-0.008257	100
IRBP2	0.7	8.37	3.099	1.425e-5	8.806e-10	417.5	-0.008243	100
IRBP3	0.7	7.03	113.9	1.432e-5	9.549e-10	417.9	-0.00304	100
Naive	0.9	1.0	0.2242	0.4134	2.246e-7	651.6	-8.297e-15	100
Bisection	0.9	35.71	15.72	2.438e-14	-1.401e-11	429.1	3.039e-7	100
IRBP1	0.9	8.36	2.378	0.0007969	9.742e-7	433.9	-0.005977	100
IRBP2	0.9	8.36	3.082	0.0007997	1.108e-6	433.9	-0.00598	100
IRBP3	0.9	6.43	77.27	0.001567	1.085e-6	433.2	-0.004778	100
Naive	0.99	1.0	0.2113	0.123	4.541e-8	457.2	8.138e-16	100
Bisection	0.99	27.52	13.22	7.071e-15	-1.258e-14	448.9	5.677e-9	100
IRBP1	0.99	9.0	2.618	0.0004196	1.962e-8	449.3	-0.0007902	100
IRBP2	0.99	9.0	3.46	0.0004194	1.954e-8	449.3	-0.0007902	100
IRBP3	0.99	7.0	83.49	0.0005736	9.499e-9	449.0	-0.0001324	100

from 50 to 1000 (incremented by 50) and the number of measurements m from 200 to 6000 (incremented by 200). We consider a sparse signal \mathbf{s} whose support (of size s) is chosen uniformly at random with i.i.d. standard normal values, and a random sensing matrix $\mathbf{A}^{m \times d}$ whose entries are i.i.d. standard normal. Noiseless measurements ($\boldsymbol{\epsilon} = \mathbf{0}$) are assumed. The radius r of the ℓ_p -ball is set to $\|\mathbf{s}\|_p$.⁶ A PGD trial with $\gamma_k = 1/m$ is stopped after 500 iterations, and recovery is declared successful if $\|\mathbf{x}^{(n)} - \mathbf{s}\|_2 / \|\mathbf{s}\|_2 < 10^{-3}$ to set the optimal solution $\hat{\mathbf{x}} = \mathbf{x}^{(n)}$. The average success rate of 50 trials for each combination of m and s is recorded.

The result, plotted in Figure 2, clearly demonstrates the phase transition phenomenon in compressed sensing; namely, for each sparsity level, there is a sharp transition of the success probability as the number of measurements increases. The success rate is higher if the signal is more sparse. This result also confirms the finding of Oymak et al. (2017) that $p = 0.5$ outperforms both $p = 1$ and $p = 0$. Among the latter two, $p = 0$ has a higher probability of success. It is interesting to note that both $p = 0.1$ and 0.9 perform slightly better than $p = 0$, and that $p = 0.3$ and 0.7 perform similarly to $p = 0.5$. Hence unlike what is predicted by the theory of Bahmani and Raj (2013), there seems a *range* of intermediate values of p away from both 0 and 1 that performs best in combination with PGD. The reason for this will be an interesting subject of further research.

⁶This optimal tuning parameter as required by the theory of Oymak et al. (2017) can be relaxed. However, we closely follow the experiment setup of Oymak et al. (2017) here.



7 Discussion

We have proposed robust and highly scalable algorithms for projecting onto ℓ_p balls in general, a key component of many learning tasks. Their merits are demonstrated empirically and agree with our theoretical treatment; our contributions outpace and outperform the limited prior work for a difficult but core computational problem, and provide a unified view of the convex and non-convex cases. These tools open the door to previously intractable penalty and constraint formulations, which have shown to be often better suited to various learning tasks than their more convenient counterparts.

References

- Argyriou, A., T. Evgeniou, and M. Pontil (2008). Convex multi-task feature learning. *Mach. Learn.* 73(3), 243–272.
- Bahmani, S. and B. Raj (2013). A unifying analysis of projected gradient descent for ℓ_p -constrained least squares. *Appl. Comput. Harmon. Anal.* 34(3), 366–378.
- Barbero, A. and S. Sra (2018). Modular proximal optimization for multidimensional total-variation regularization. *J. Mach. Learn. Res.* 19(1), 2232–2313.
- Beck, A. and M. Teboulle (2009). A fast iterative shrinkage-thresholding algorithm for linear inverse problems. *SIAM J. Imaging Sci.* 2(1), 183–202.
- Bertsekas, D. (1999). *Nonlinear Programming* (2nd ed.). Belmont, Mass., USA: Athena Scientific.
- Bertsekas, D. P. (1982). Projected Newton methods for optimization problems with simple constraints. *SIAM J. Control Optim.* 20(2), 221–246.
- Blumensath, T. and M. E. Davies (2009). Iterative hard thresholding for compressed sensing. *Appl. Comput. Harmon. Anal.* 27(3), 265–274.
- Boyd, S. P. and L. Vandenberghe (2004). *Convex optimization*. Cambridge, UK: Cambridge University Press.
- Candes, E. J. and T. Tao (2005). Decoding by linear programming. *IEEE Tran. Inform. Theory* 51(12), 4203–4215.
- Chartrand, R. and V. Staneva (2008). Restricted isometry properties and nonconvex compressive sensing. *Inverse Problems* 24(3), 035020.
- Chartrand, R. and W. Yin (2016). Nonconvex sparse regularization and splitting algorithms. In *Splitting Methods in Communication, Imaging, Science, and Engineering*, pp. 237–249. Springer.
- Chen, L., X. Jiang, X. Liu, T. Kirubarajan, and Z. Zhou (2021). Outlier-robust moving object and background decomposition via structured ℓ_p -regularized low-rank representation. *IEEE Trans. Emerg. Topics Comput. Intell.* 5, 620–638.
- Chen, X., L. Niu, and Y. Yuan (2013). Optimality conditions and a smoothing trust region newton method for nonlipschitz optimization. *SIAM J. Optim.* 23(3), 1528–1552.

- Condat, L. (2016). Fast projection onto the simplex and the ℓ_1 ball. *Math. Program.* 158(1-2), 575–585.
- Das Gupta, M. and S. Kumar (2013). Non-convex p-norm projection for robust sparsity. In *Proc. IEEE Int. Conf. Computer Vision*, pp. 1593–1600.
- Donoho, D. L. (2006). Compressed sensing. *IEEE Tran. Inform. Theory* 52(4), 1289–1306.
- Duchi, J., S. Shalev-Shwartz, Y. Singer, and T. Chandra (2008). Efficient projections onto the ℓ_1 -ball for learning in high dimensions. In *Proc. 25th Int. Conf. Mach. Learn.*, pp. 272–279. ACM.
- Fu, W. J. (1998). Penalized regressions: the bridge versus the lasso. *J. Comput. Graph. Statist.* 7(3), 397–416.
- Hu, Y., C. Li, K. Meng, J. Qin, and X. Yang (2017). Group sparse optimization via $\ell_{p,q}$ regularization. *J. Mach. Learn. Res.* 18(1), 960–1011.
- Lange, K. (2016). *MM Optimization Algorithms*. Philadelphia, PA, USA: SIAM.
- Liu, H., M. Palatucci, and J. Zhang (2009). Blockwise coordinate descent procedures for the multi-task lasso, with applications to neural semantic basis discovery. In *Proc. 26th Int. Conf. Mach. Learn.*, pp. 649–656. ACM.
- Liu, J., S. Ji, and J. Ye (2011). SLEP: Sparse learning with efficient projections. Technical report, Arizona State University.
- Liu, J. and J. Ye (2010). Efficient ℓ_1/ℓ_q norm regularization. *arXiv preprint arXiv:1009.4766*.
- Lu, Z. (2014). Iterative reweighted minimization methods for ℓ_p regularized unconstrained nonlinear programming. *Math. Program.* 147(1), 277–307.
- Marjanovic, G. and V. Solo (2012). On ℓ_q optimization and matrix completion. *IEEE Trans. Signal Process.* 60(11), 5714–5724.
- Meier, L., S. Van De Geer, and P. Bühlmann (2008). The group lasso for logistic regression. *J. R. Stat. Soc. Ser. B. Stat. Methodol.* 70(1), 53–71.
- Oymak, S., B. Recht, and M. Soltanolkotabi (2017). Sharp time–data tradeoffs for linear inverse problems. *IEEE Tran. Inform. Theory* 64(6), 4129–4158.
- Quattoni, A., X. Carreras, M. Collins, and T. Darrell (2009). An efficient projection for $\ell_{1,\infty}$ regularization. In *Proc. 26th Int. Conf. Mach. Learn.*, pp. 857–864. ACM.
- Sattar, Y. and S. Oymak (2020). Quickly finding the best linear model in high dimensions via projected gradient descent. *IEEE Trans. Signal Process.* 68, 818–829.
- Sra, S. (2012). Fast projections onto mixed-norm balls with applications. *Data Min. Knowl. Discov.* 25(2), 358–377.
- Tibshirani, R., M. Wainwright, and T. Hastie (2015). *Statistical learning with sparsity: the lasso and generalizations*. Chapman and Hall/CRC.
- Vogt, J. E. and V. Roth (2012). A complete analysis of the $\ell_{1,p}$ group-lasso. In *Proc. 29th Int. Conf. Mach. Learn.*, pp. 1091–1098. Omnipress.

- Wang, M., W. Xu, and A. Tang (2011). On the performance of sparse recovery via ℓ_p -minimization ($0 \leq p \leq 1$). *IEEE Tran. Inform. Theory* 57(11), 7255–7278.
- Xu, Z., X. Chang, F. Xu, and H. Zhang (2012). $L_{1/2}$ regularization: a thresholding representation theory and a fast solver. *IEEE Trans. Neural Netw. Learn. Syst.* 23(7), 1013–1027.
- Yang, X., J. Wang, and H. Wang (2021). Towards an efficient approach for the nonconvex ℓ_p ball projection: algorithm and analysis. *arXiv preprint arXiv:2101.01350*.
- Yuan, M. and Y. Lin (2006). Model selection and estimation in regression with grouped variables. *J. R. Stat. Soc. Ser. B. Stat. Methodol.* 68(1), 49–67.
- Yukawa, M. and S.-i. Amari (2016). ℓ_p -regularized least squares ($0 < p < 1$) and critical path. *IEEE Trans. Inform. Theory* 62(1), 488–502.
- Zhang, Y., D.-Y. Yeung, and Q. Xu (2010). Probabilistic multi-task feature selection. In *Adv. Neural Inf. Process. Syst.*, pp. 2559–2567.
- Zhou, Z., Q. Zhang, and A. M.-C. So (2015). $\ell_{1,p}$ -norm regularization: Error bounds and convergence rate analysis of first-order methods. In *Proc. 32nd Int. Conf. Mach. Learn.*, Volume 37, pp. 1501–1510.

Algorithm 2 Dual Newton ascent

Input: $\mathbf{y} > 0$ with $\|\mathbf{y}\|_p > 1$, $p > 1$

$q \leftarrow p/(p-1)$

Choose $\mu \in (0, \|\mathbf{y}\|_q]$; $\alpha \in (0, 1/2)$; $\beta \in (0, 1)$

Main loop:

repeat

$\Delta\mu \leftarrow -g'(\mu)/g''(\mu)$

$t \leftarrow 1$

while $g(\mu + t\Delta\mu) < g(\mu) + \alpha tg'(\mu)\Delta\mu$ **do** {Armijo rule}

$t \leftarrow \beta t$

end while

$\mu \leftarrow \mu + t\Delta\mu$

until convergence

$\mathbf{x}^* \leftarrow (\text{prox}_{\mu s_p}(y_1), \dots, \text{prox}_{\mu s_p}(y_d))^T$ {eq. (8)}

return \mathbf{x}^*

Algorithm 3 Dual bisection

Input: $\mathbf{y} > 0$ with $\|\mathbf{y}\|_p > 1$, $p > 0$

$q^* \leftarrow p/(p-1)$ if $p \neq 1$, $q^* = \infty$ if $p = 1$

$(\mu_l, \mu_r) \leftarrow (0, \|\mathbf{y}\|_{q^*})$

repeat

$\mu_m \leftarrow (\mu_l + \mu_r)/2$

if $(r(\mu_l) - 1)(r(\mu_m) - 1) < 0$ **then** {eq. (16)}

$\mu_r \leftarrow \mu_m$

else

$\mu_l \leftarrow \mu_m$

end if

until convergence

$\mathbf{x}^* \leftarrow (\text{prox}_{\mu_m s_p}(y_1), \dots, \text{prox}_{\mu_m s_p}(y_d))^T$ {eq. (8)}

return \mathbf{x}^*
